SUPPORTING INFORMATION FILE

Thermoelectric properties of $In_1Co_4Sb_{12+\delta}$: role of *in situ* formed InSb precipitates, Sb overstoichiometry, and processing conditions

Alexandra Ivanova,[a,*,#] Andrei Novitskii,[a,b,#] Illia Serhiienko,[b,c,#] Gabin Guélou,[b,‡] Tatyana Sviridova,[a] Sergey Novikov,[d] Mikhail Gorshenkov,[a] Aleksei Bogach,[e] Andrey Korotitskiy,[a] Andrei Voronin,[a] Alexander Burkov,[d] Takao Mori[b,c] and Vladimir Khovaylo[a,f]

[a.] National University of Science and Technology MISIS (NUST MISIS), Leninsky av. 4, Moscow, 119049, Russia.
[b.] International Center for Materials Nanoarchitectonics (WPI-MANA), National Institute for Materials Science (NIMS), 1-1 Namiki, Ibaraki, Tsukuba, 305-0044, Japan.
[c.] Graduate School of Pure and Applied Sciences, University of Tsukuba, 1-1-1 Tennodai, Ibaraki, Tsukuba, 305-8573, Japan.
[d.] Ioffe Institute, Politekhnicheskaya st. 26, Saint Petersburg, 194021, Russia.
[e.] Prokhorov General Physics Institute of the Russian Academy of Sciences, Vavilova st. 38, Moscow, 119991, Russia.
[f.] Belgorod State University, Pobedy st. 85, Belgorod, 308015, Russia.
§ Electronic Supplementary Information (ESI) is available.
* Corresponding author. E-mail address: m154566@edu.misis.ru (A. Ivanova).
‡ Present address: CRISMAT, CNRS, Normandie University, ENSICAEN, UNICAEN, 14000 Caen, France.
# These authors contribute equally to the paper.

Scheme of the fabrication route for the samples under study

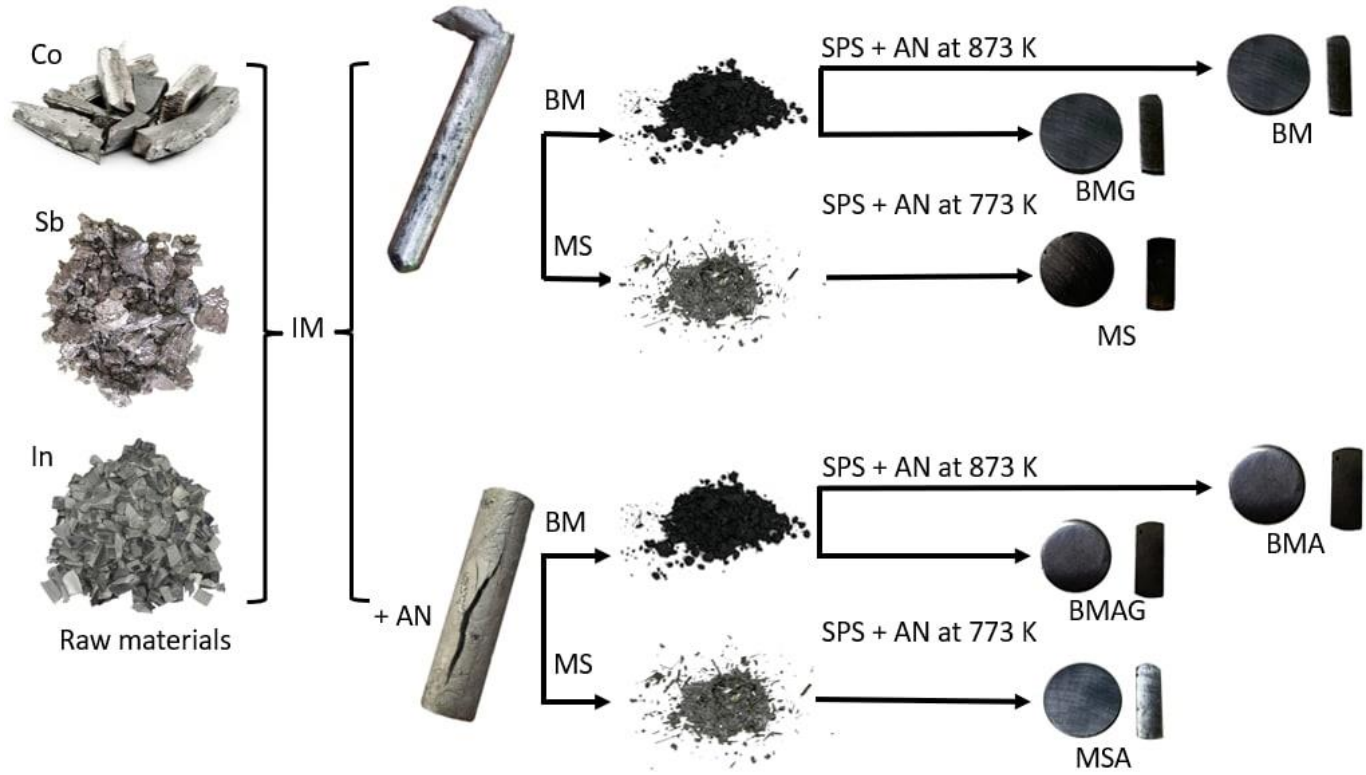

Figure S1. Schematic illustration of the fabrication routes for the In-filled skutterudites with a nominal composition of $In_1Co_4Sb_{12+\delta}$. Here IM is the induction melting, AN is the annealing, BM is the ball milling, MS is the melt spinning, and SPS is the spark plasma sintering.

XRD data for all the samples before sintering

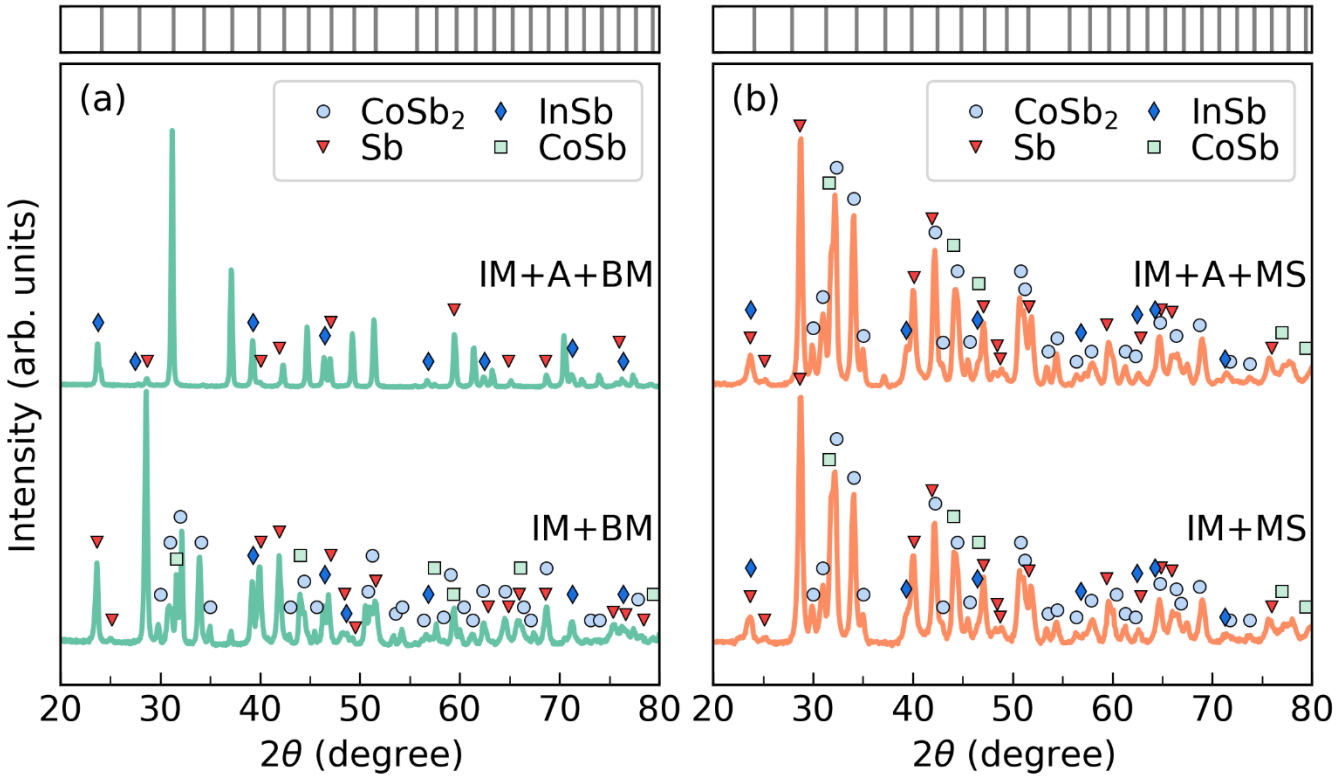

Figure S2. PXRD patterns for the samples with a nominal composition of $In_1Co_4Sb_{12+\delta}$ before spark plasma sintering after (a) induction melting and ball milling (IM + BM), induction melting, annealing and ball milling (IM + A + BM), (b) induction melting and melt spinning (IM + MS), induction melting, annealing and melt spinning (IM + A + MS). Bragg's reflections for the $CoSb_3$ phase are indicated by ticks on the top part of the figure. The first and the second sets of samples were obtained by sintering the powders whose XRD patterns are shown in (a). The third set of samples was fabricated by sintering the ribbons whose XRD patterns are shown in (b).

Table S1. The phase composition of the samples with a nominal composition of $In_1Co_4Sb_{12+\delta}$ before spark plasma sintering according to the XRD pattern refinement.

Phase	Route*							
	IM + BM		IM + A + BM		IM + MS		IM + A + MS	
	Content (vol.%)	Lattice parameters (Å)	Content (vol.%)	Lattice parameters (Å)	Content (vol.%)	Lattice parameters (Å)	Content (vol.%)	Lattice parameters (Å)
$CoSb_3$	5.7	a = 9.042	80.3	a = 9.051	0	n/a	3.6	a = 9.050
$CoSb_2$	27.8	a = 5.577 b = 6.385 c = 3.375	0	n/a	40.9	a = 5.587 b = 6.391 c = 3.367	41.7	a = 5.588 b = 6.391 c = 3.369
CoSb	9.5	a = 3.869 c = 5.194	0	n/a	15.7	a = 3.852 c = 5.202	12.3	a = 3.853 c = 5.200
InSb	14.8	a = 6.475	17.2	a = 6.479	4.6	a = 6.466	5.7	a = 6.465
Sb	42.2	a = 4.296 c = 11.298	2.5	–	38.8	a = 4.279 c = 11.316	36.7	a = 4.279 c = 11.318

*According to labels depicted in Figure S2.

Rietveld refinements

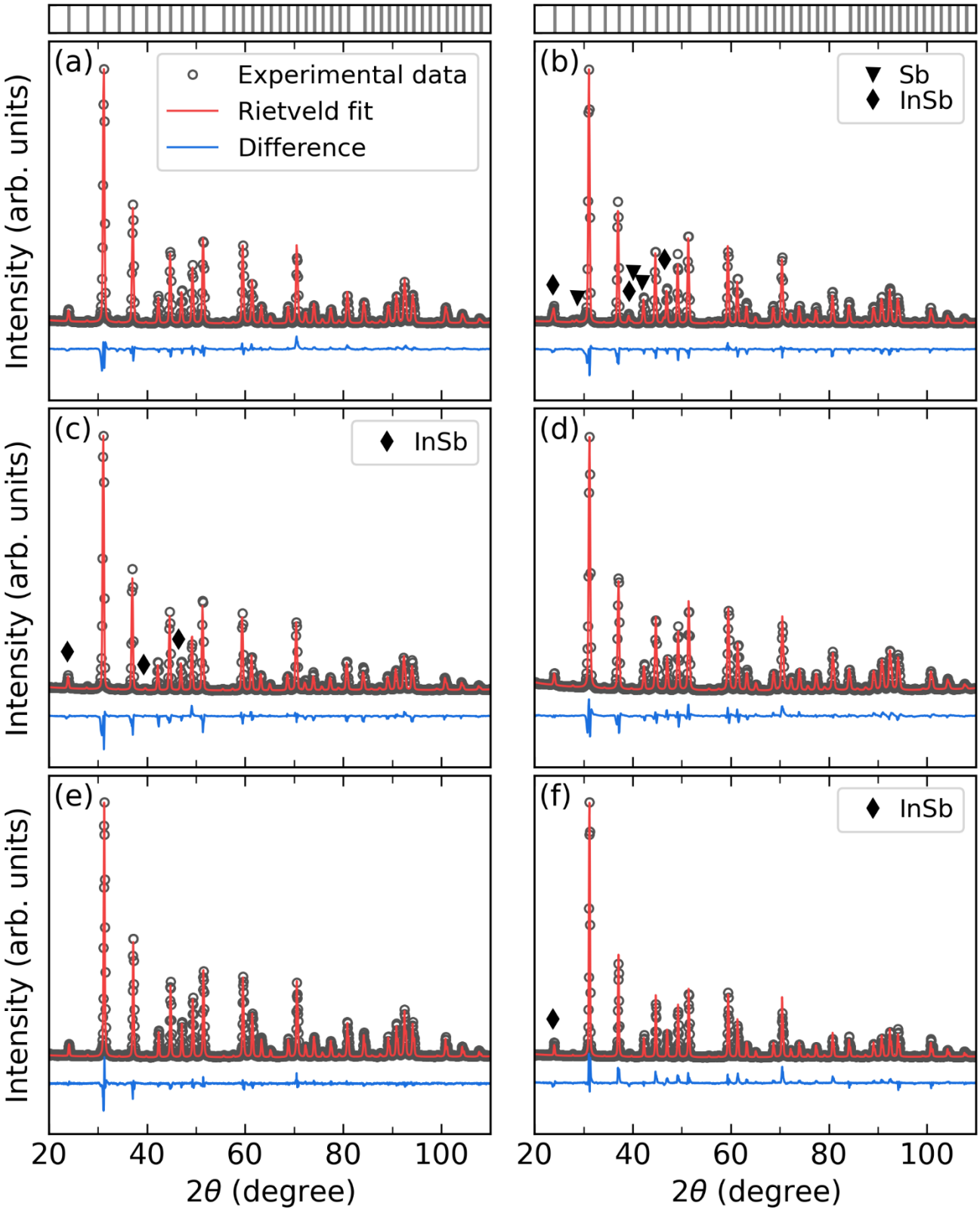

Figure S3. Rietveld refinements for the (a) BMG, (b) BMAG, (c) MS, (d) MSA, (e) BM, and (f) BMA samples after spark plasma sintering and annealing. Bragg's reflections for the $CoSb_3$ phase are indicated by ticks on the top part of the figure.

Table S2. Reliability factors of the refined spectra shown in Fig. S3: intensity *R*-factor, R_p, weighted profile *R*-factor, R_{wp}, expected *R*-factor, R_{exp}, and goodness of fit, *GoF* (=R_{wp}/R_{exp}).

Sample code	R_p (%)	R_{wp} (%)	R_{exp} (%)	*GoF*
BMG	8.3	11.7	2.5	4.7
BMAG	7.6	10.1	2.8	3.6
MS	9.0	12.6	2.9	4.3
MSA	7.9	10.9	3.3	3.3
BM	9.1	12.0	10.1	1.2
BMA	10.4	14.8	8.0	1.9

Here $R_{de} = \frac{\max\left(y_{obs,i} - y_{calc,i}\right)}{\max\left(y_{obs,i}\right)}$, $R_p = \frac{\sum_{i=1}^{N}\left|y_{obs,i} - y_{calc,i}\right|}{\sum_{i=1}^{N} y_{obs,i}}$, $R_{wp} = \sqrt{\frac{\sum_{i=1}^{N} w_i\left(y_{obs,i} - y_{calc,i}\right)^2}{\sum_{i=1}^{N} w_i y_{obs,i}^2}}$, and $R_{exp} = \sqrt{\frac{N-P}{\sum_{i=1}^{N} w_i y_{obs,i}^2}}$, where $y_{obs,i}$ is the observed (experimental) intensity, $y_{calc,i}$ is the calculated intensity, w_i is the weight, N is the number of data points, and P is the number of refined parameters (for all the samples $P \approx 20$ and thus $N \gg P$).

Table S3. Crystal structure data for all the phases mentioned in this study (Fig. 1, Fig. S2).

Phase	Pearson symbol	Space group	Structure type	Structure type in *Strukturbericht* notation	PDF card number
$CoSb_3$	cI32	$Im\bar{3}$	As_3Co	$D0_2$	65-3144
$CoSb_2$	oP6	$Pnnm$	FeS_2	C18	89-4869
CoSb	hP4	$P6_3/mmc$	NiAs	$B8_1$	65-8979
InSb	cF8	$F\bar{4}3m$	ZnS	B3	65-4817
Sb	hR2	$R\bar{3}m$	αAs	A7	76-8600

EBSD analysis

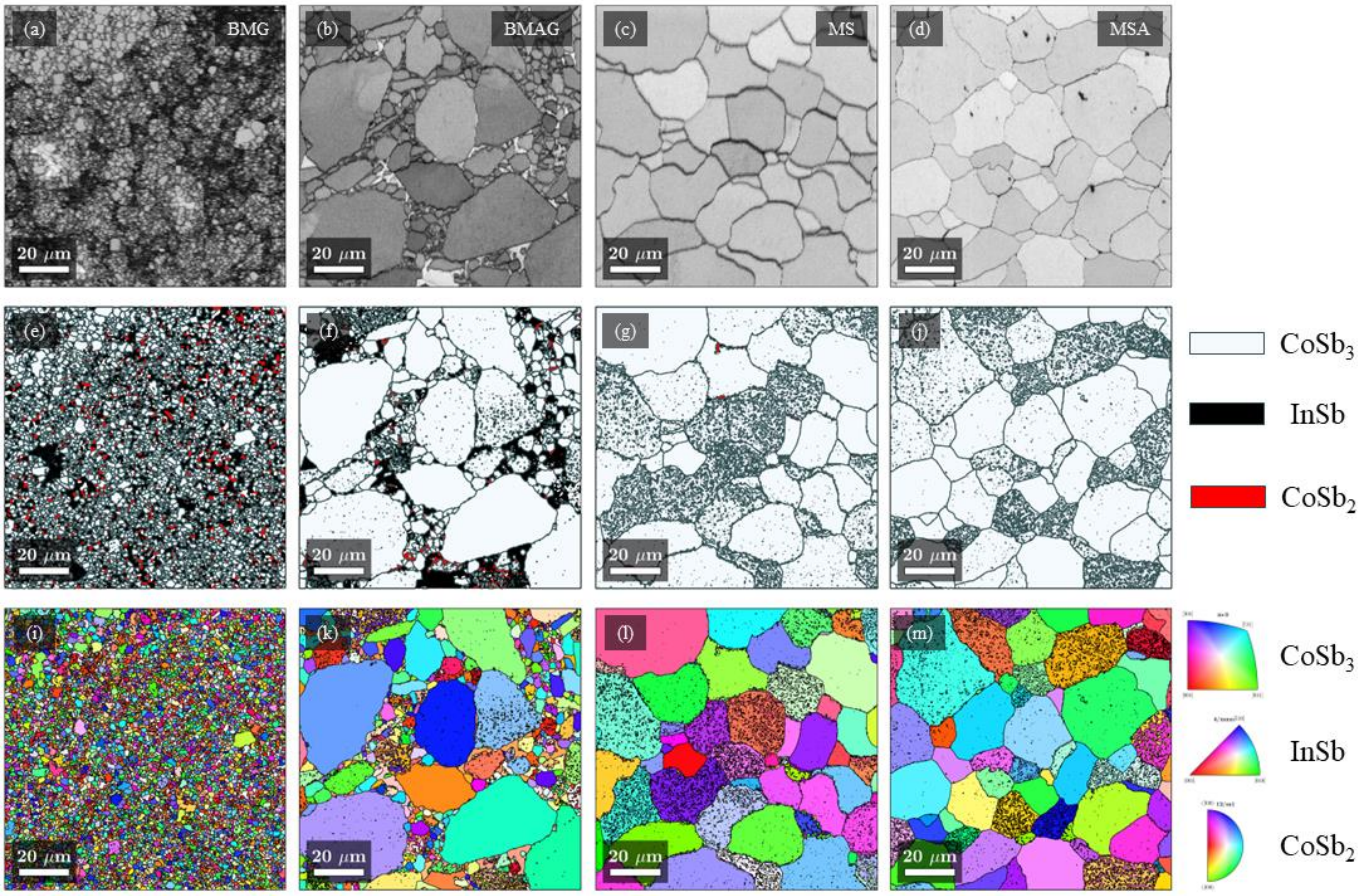

Figure S4. EBSD microstructures of the $In_1Co_4Sb_{12+\delta}$ samples prepared by various methods: (a – d) band contrast images; (e – j) phase contrast images with $CoSb_3$ phase in pale blue color, InSb in black and $CoSb_2$ in red color; (i – m) orientational contrast images for BMG (a, e, i), BMAG (b, f, k), MS (c, g, l), and MSA (d, j, m) samples, respectively.

Table S4. Calculated from the EBSD data average grain size D_g and grain boundaries length *GB* for the $In_1Co_4Sb_{12+\delta}$ samples prepared by various methods.

Property	Samples' codes			
	BMG	BMAG	MS	MSA
Average grain size D_g (μm)	6.0	20.3	9.6	10.4
Grain boundaries length *GB* (μm)	23738	8401	9452	8956

SEM images of the fracture surfaces

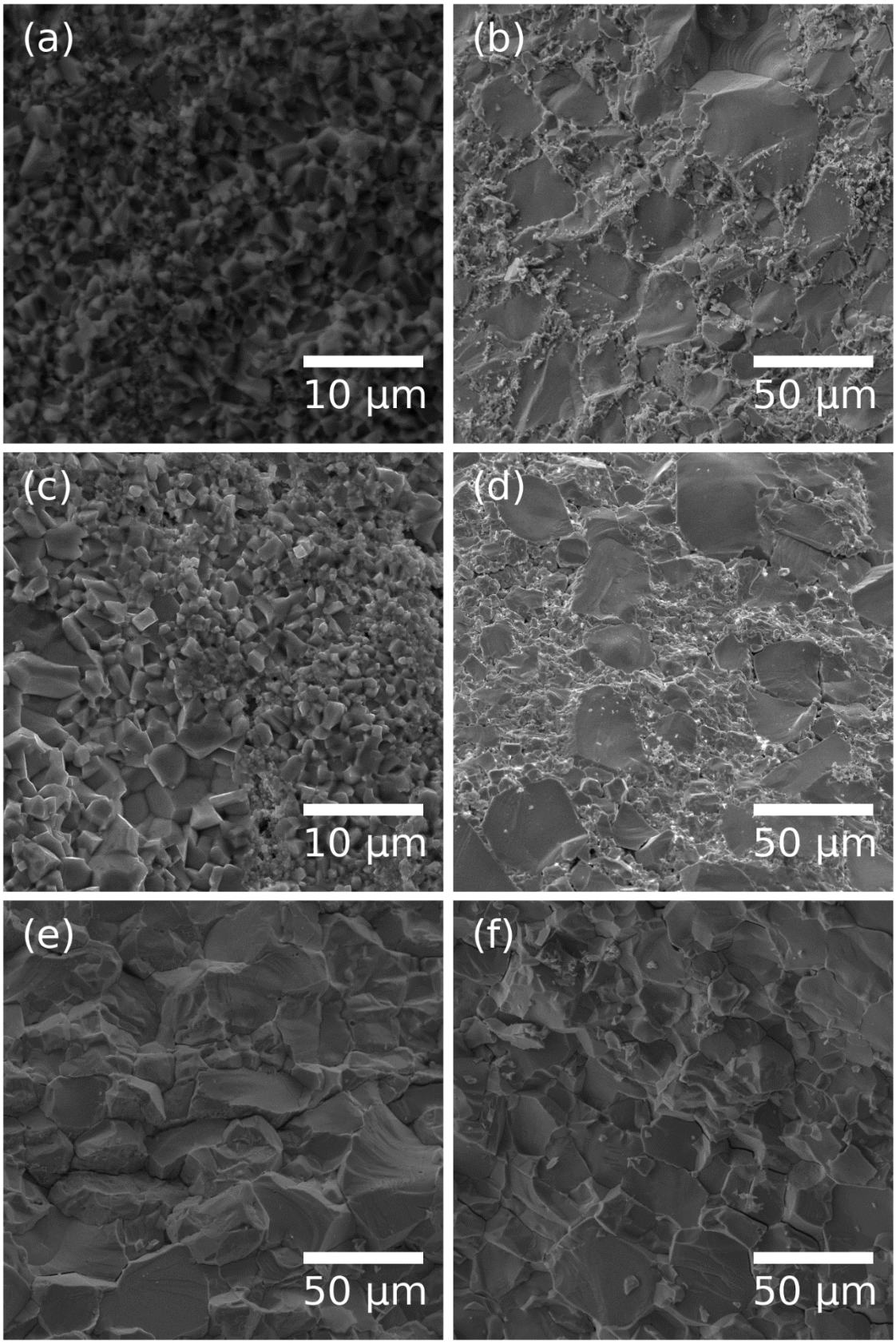

Figure S5. SEM images of the fracture surfaces of the (a) BMG, (b) BMAG, (c) BM, (d) BMA, (e) MS, and (f) MSA samples after spark plasma sintering and annealing.

EDX mapping for the BMG and BMAG samples

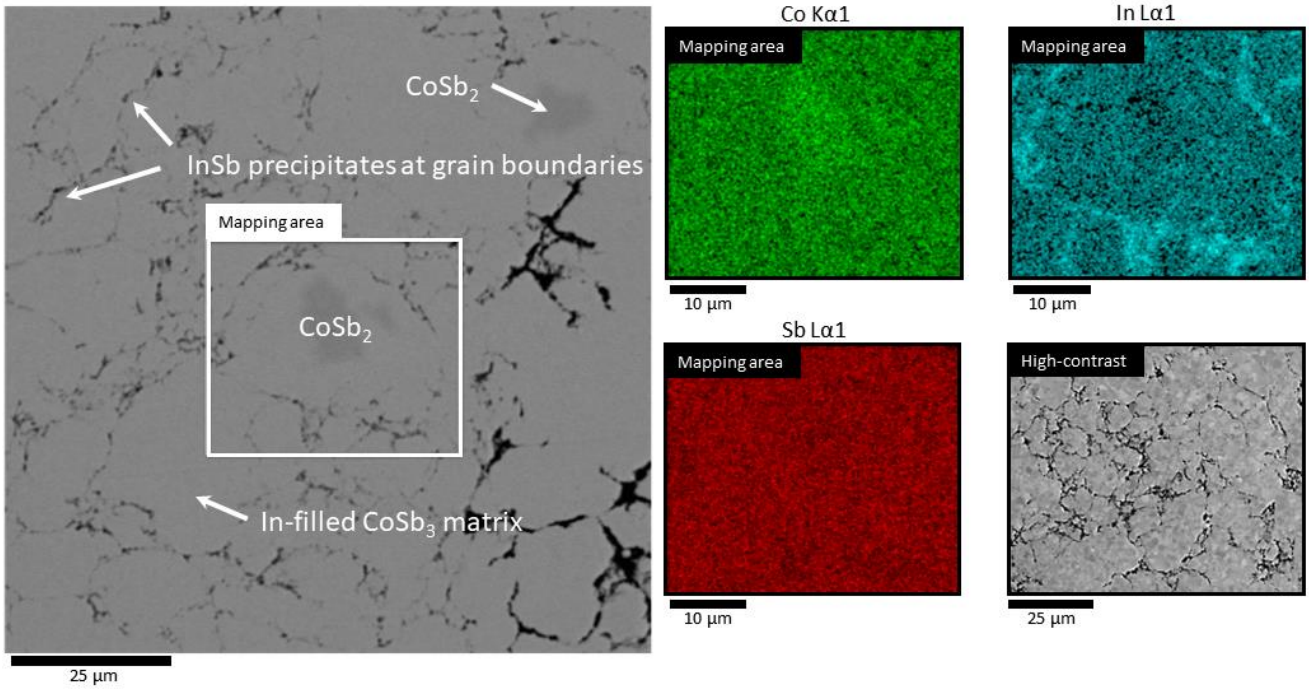

Figure S6. SEM image of the polished surface of the BMG specimen and corresponding EDX maps of the area indicated by the white rectangle. SEM micrograph in electron channeling contrast mode is also shown in the lower right corner.

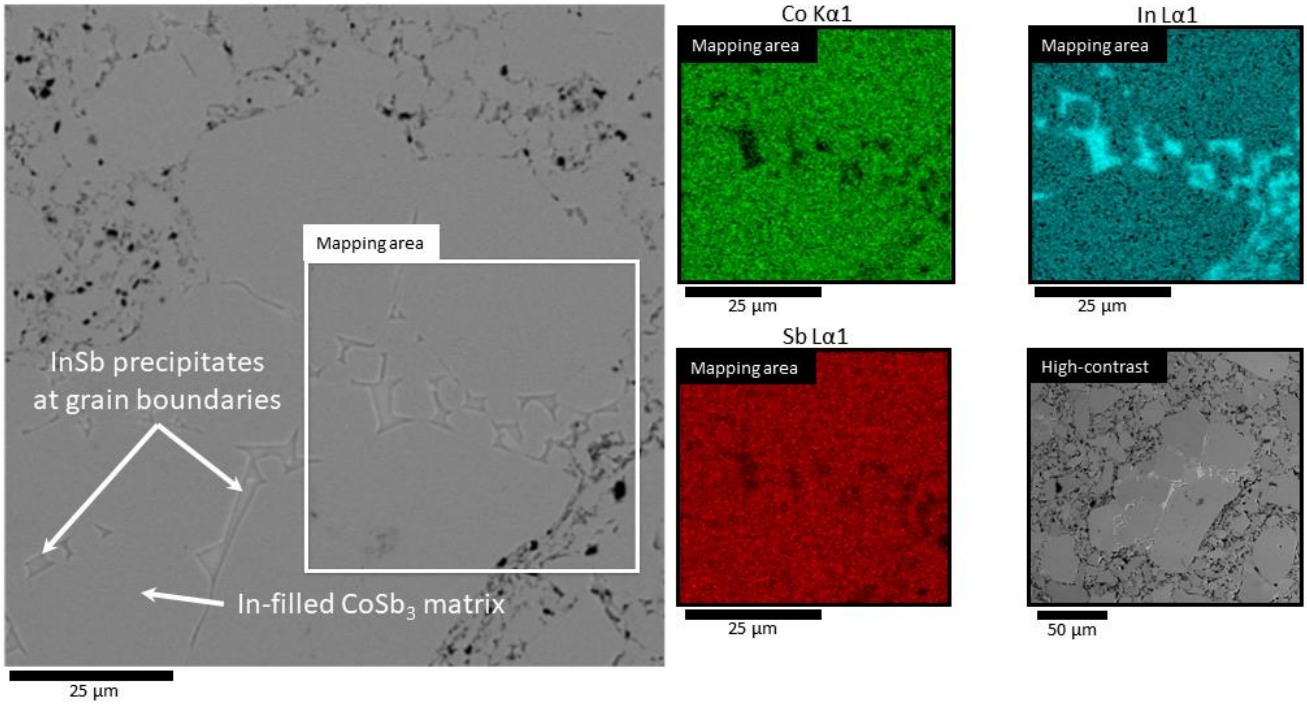

Figure S7. SEM image of the polished surface of the BMAG specimen and corresponding EDX maps of the area indicated by the white rectangle. SEM micrograph in electron channeling contrast mode is also shown in the lower right corner.

Electron diffraction patterns and representative EDX spectrum for the precipitates shown in Fig. 2c,f

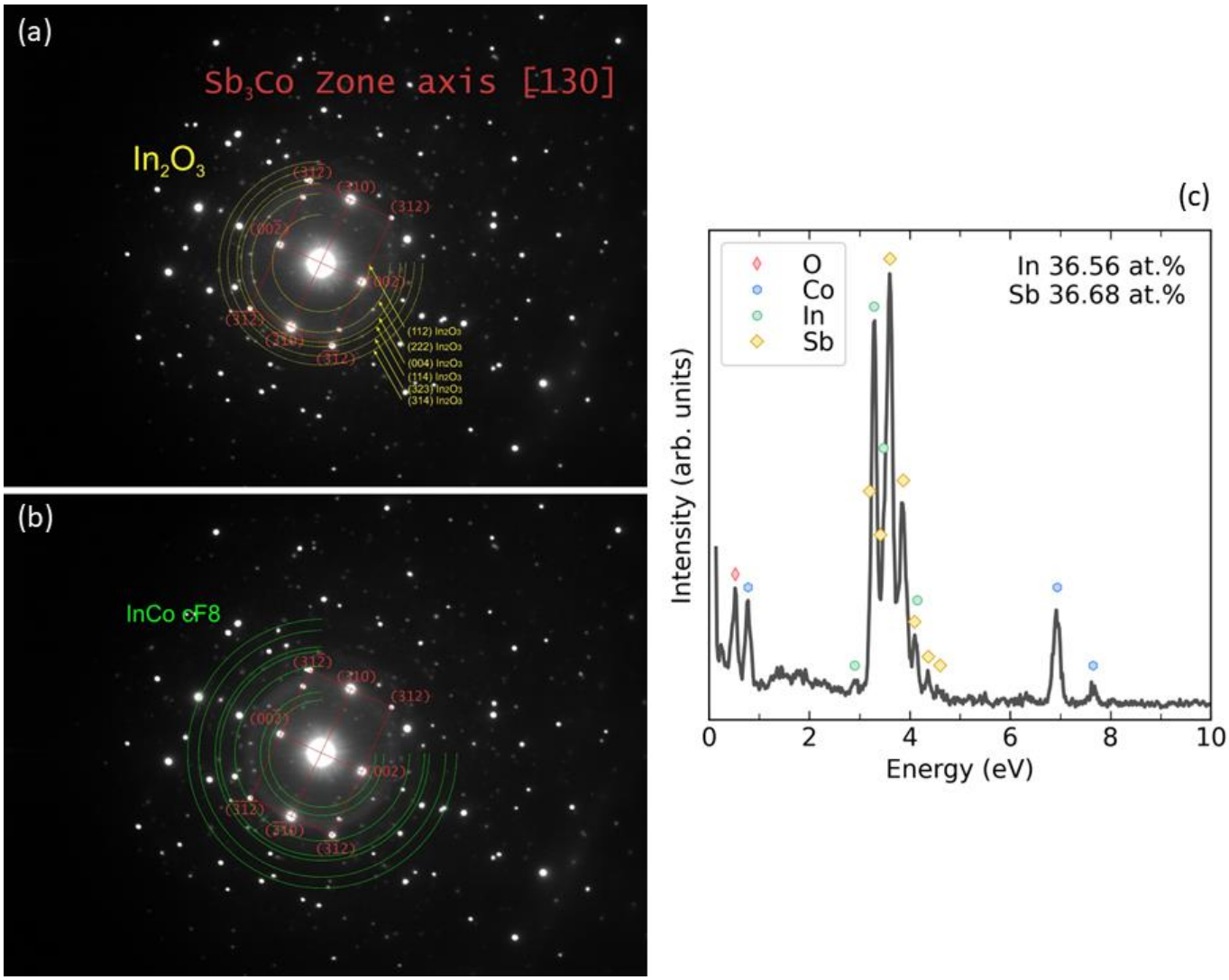

Figure S8. (a, b) Indexed electron diffraction patterns for the precipitates shown in Fig. 2c and (c) representative EDX spectrum of the inclusions shown in Fig. 2f in the main text.

EDX mapping for the BM and BMA samples

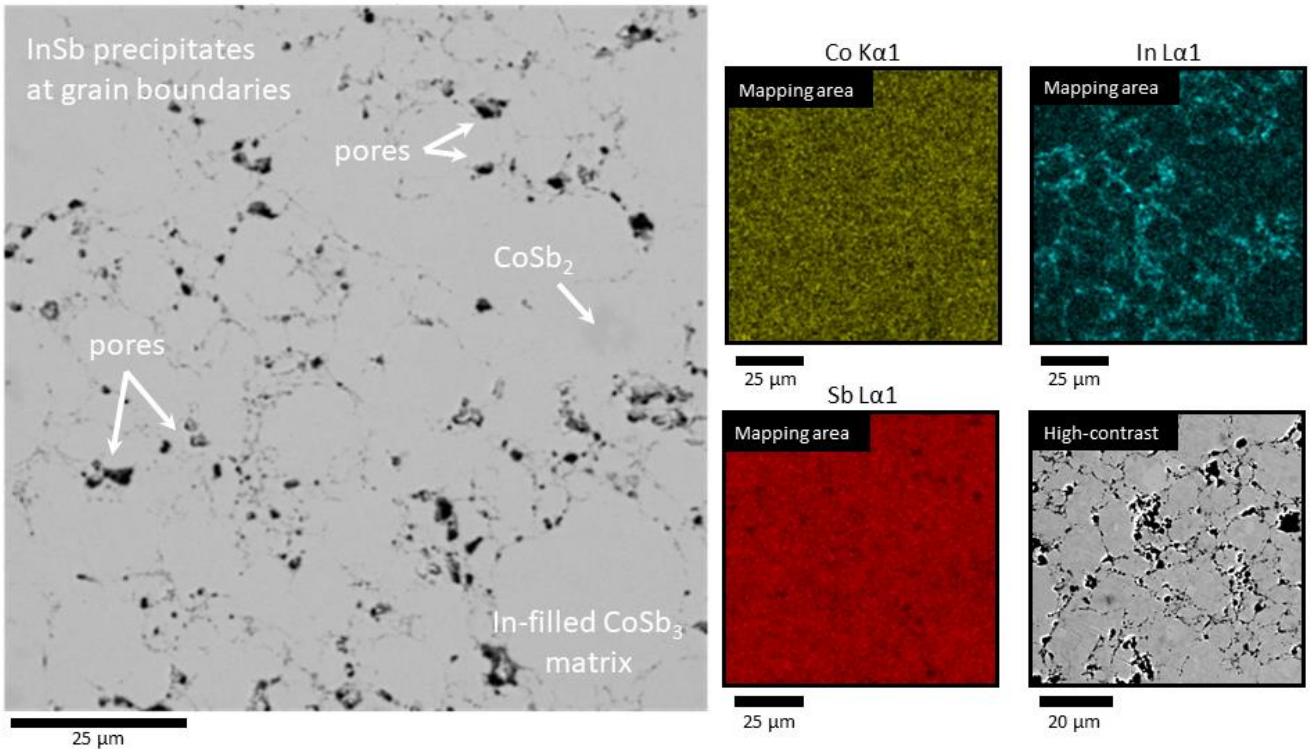

Figure S9. SEM image of the polished surface of the BM specimen and corresponding EDX maps. SEM micrograph in electron channeling contrast mode is also shown in the lower right corner.

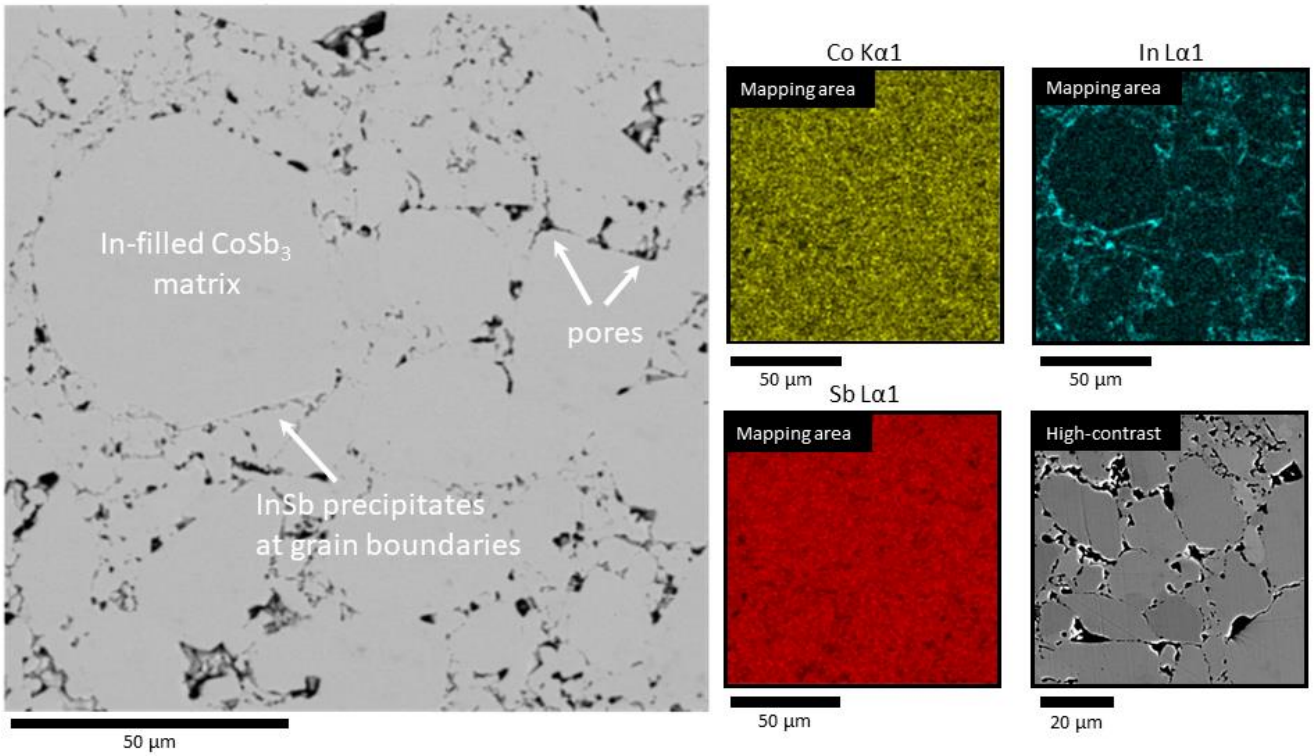

Figure S10. SEM image of the polished surface of the BMA specimen and corresponding EDX maps. SEM micrograph in electron channeling contrast mode is also shown in the lower right corner.

EDX mapping for the MS and MSA samples

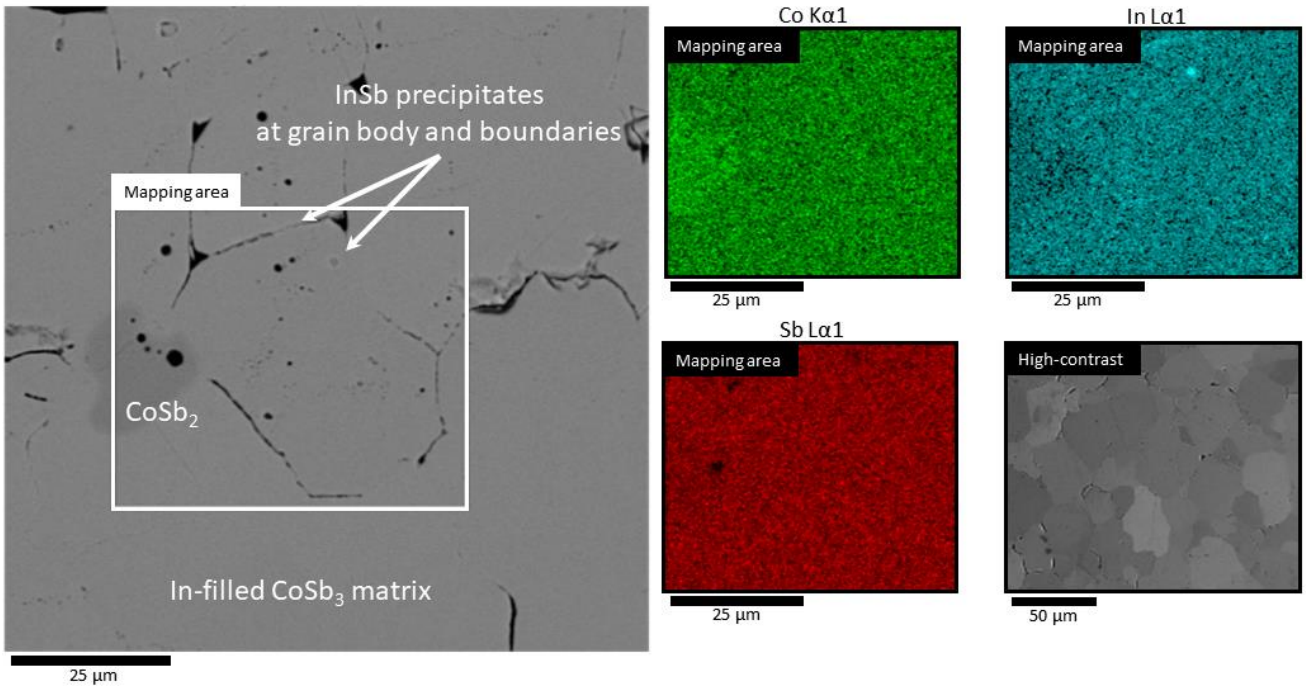

Figure S11. SEM image of the polished surface of the MS specimen and corresponding EDX maps of the area indicated by the white rectangle. SEM micrograph in electron channeling contrast mode is also shown in the lower right corner.

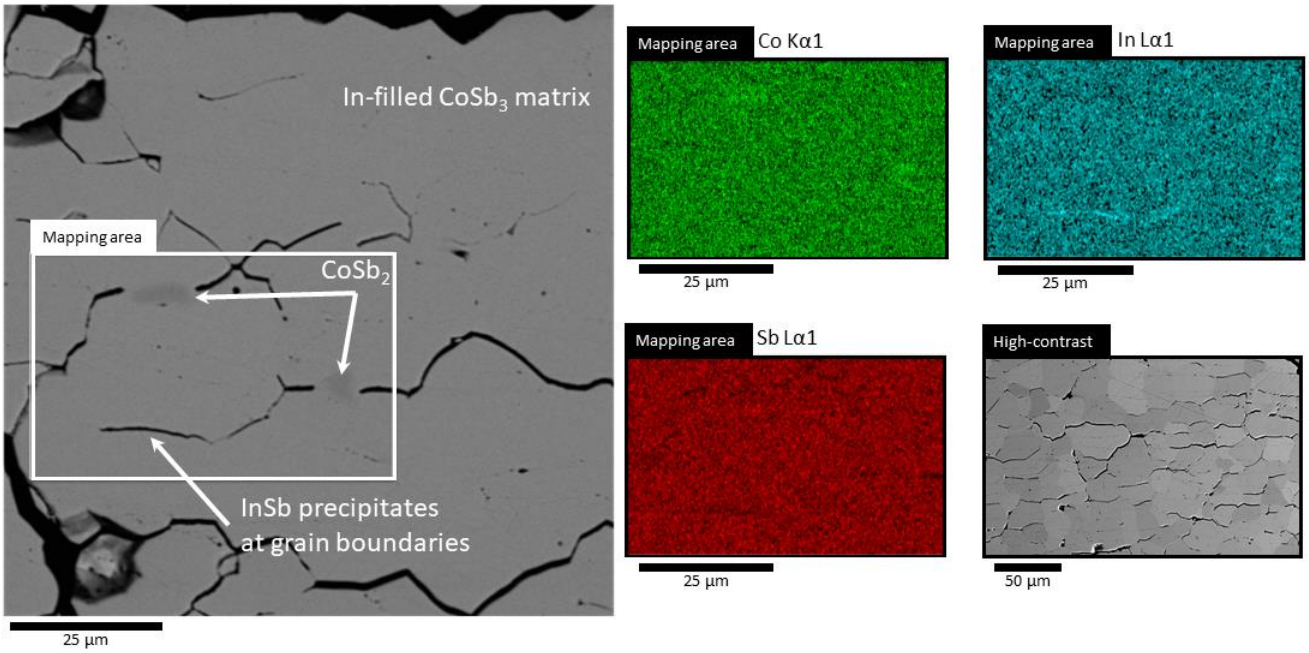

Figure S12. SEM image of the polished surface of the MSA specimen and corresponding EDX maps of the area indicated by the white rectangle. SEM micrograph in electron channeling contrast mode is also shown in the lower right corner.

Thermoelectric properties; comparison with previous reports

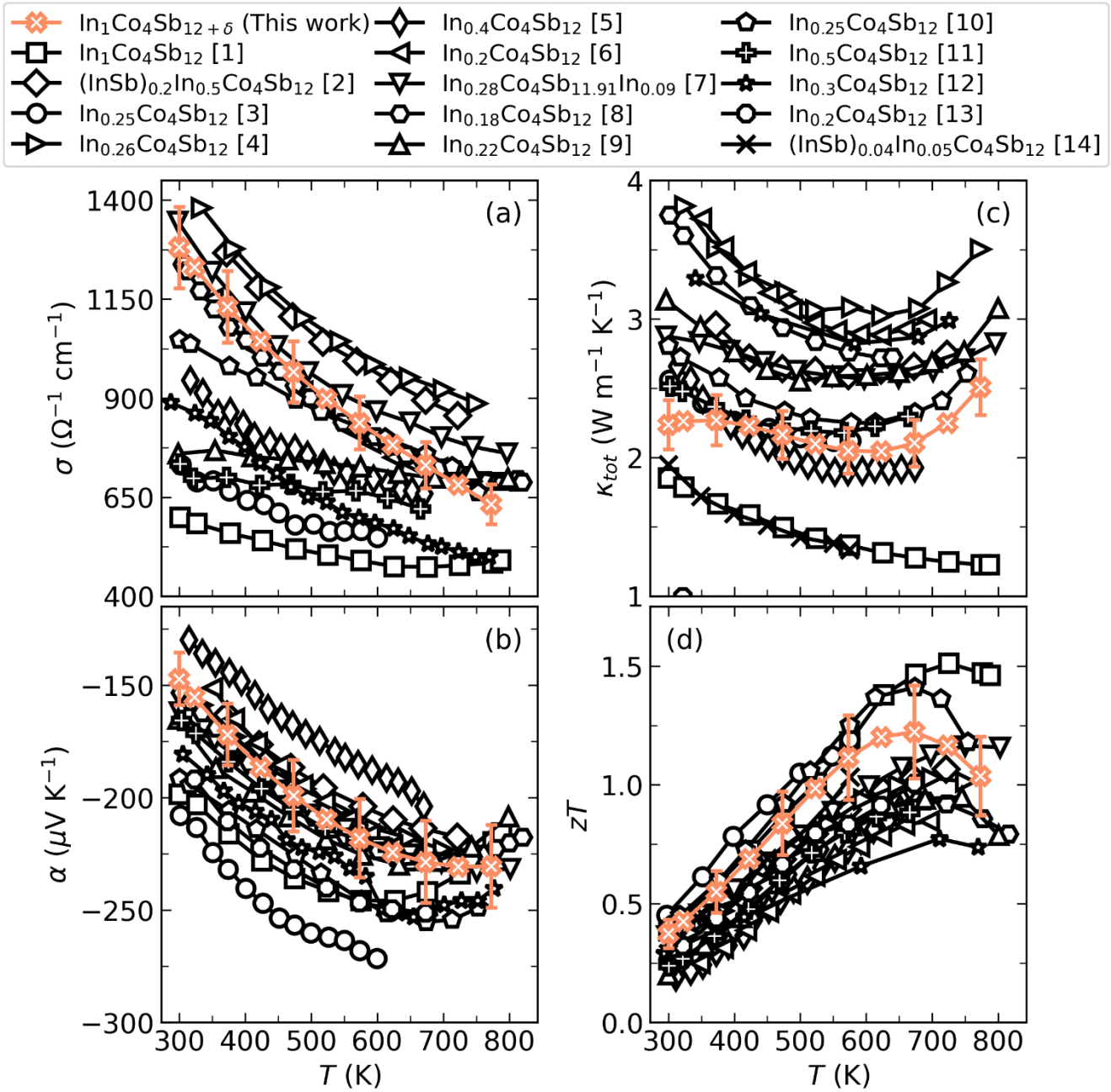

Figure S13. (a) Electrical conductivity, σ, (b) Seebeck coefficient, α, (c) total thermal conductivity, κ_{tot}, and (d) figure of merit, zT, for the $In_1Co_4Sb_{12+\delta}$ obtained in this work (MSA route) and for other In-filled $CoSb_3$ skutterudites presented for comparison.[1–14]

Field and angular dependencies of the Hall resistance

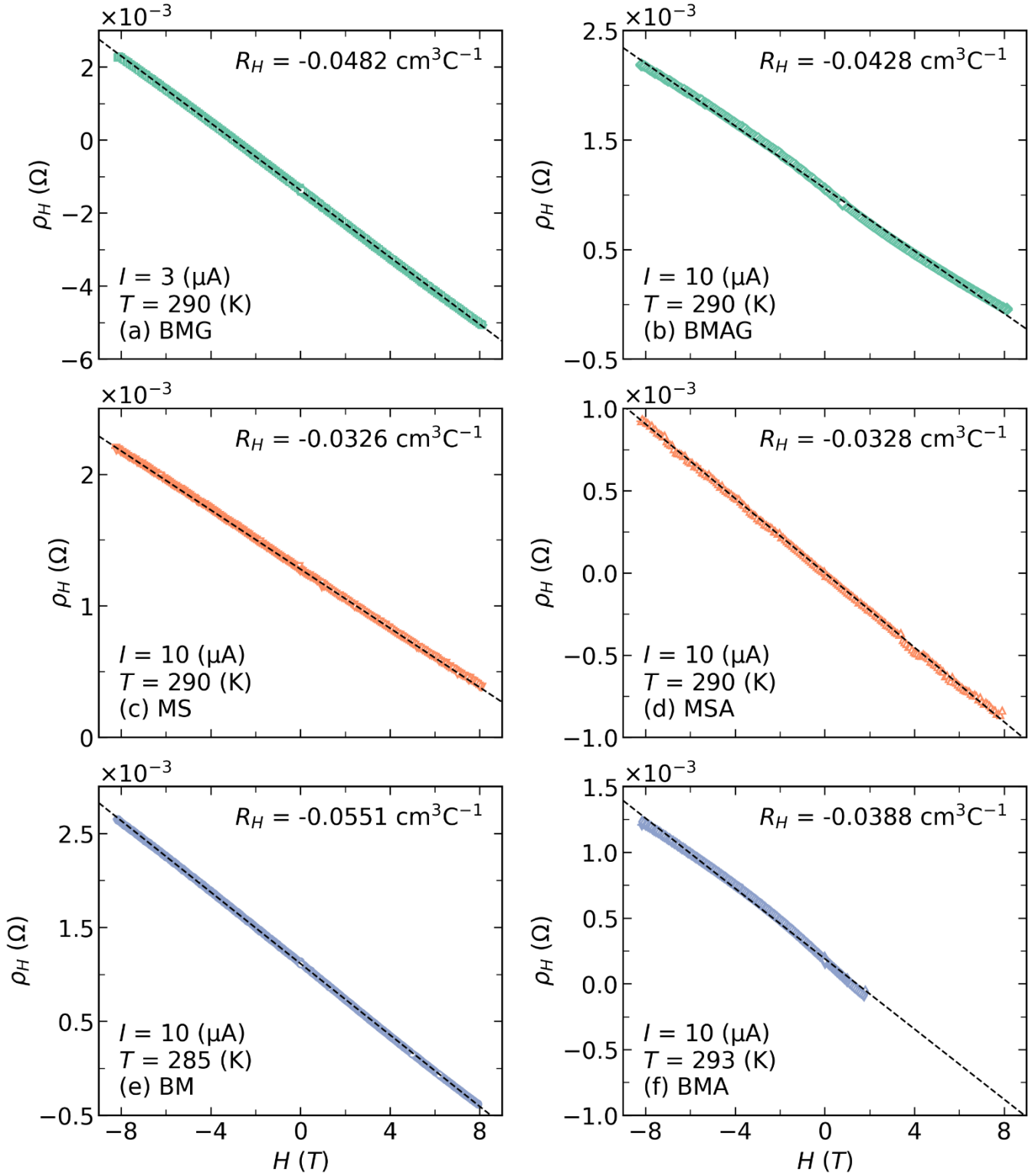

Figure S14. Magnetic field dependence of the Hall resistance for the (a) BMG, (b) BMAG, (c) MS, (d) MSA, (e) BM, and (f) BMA samples. Empty symbols are the experimentally measured points; black dashed lines are the linear fit. Here, R_H is determined from the slope of the obtained line.

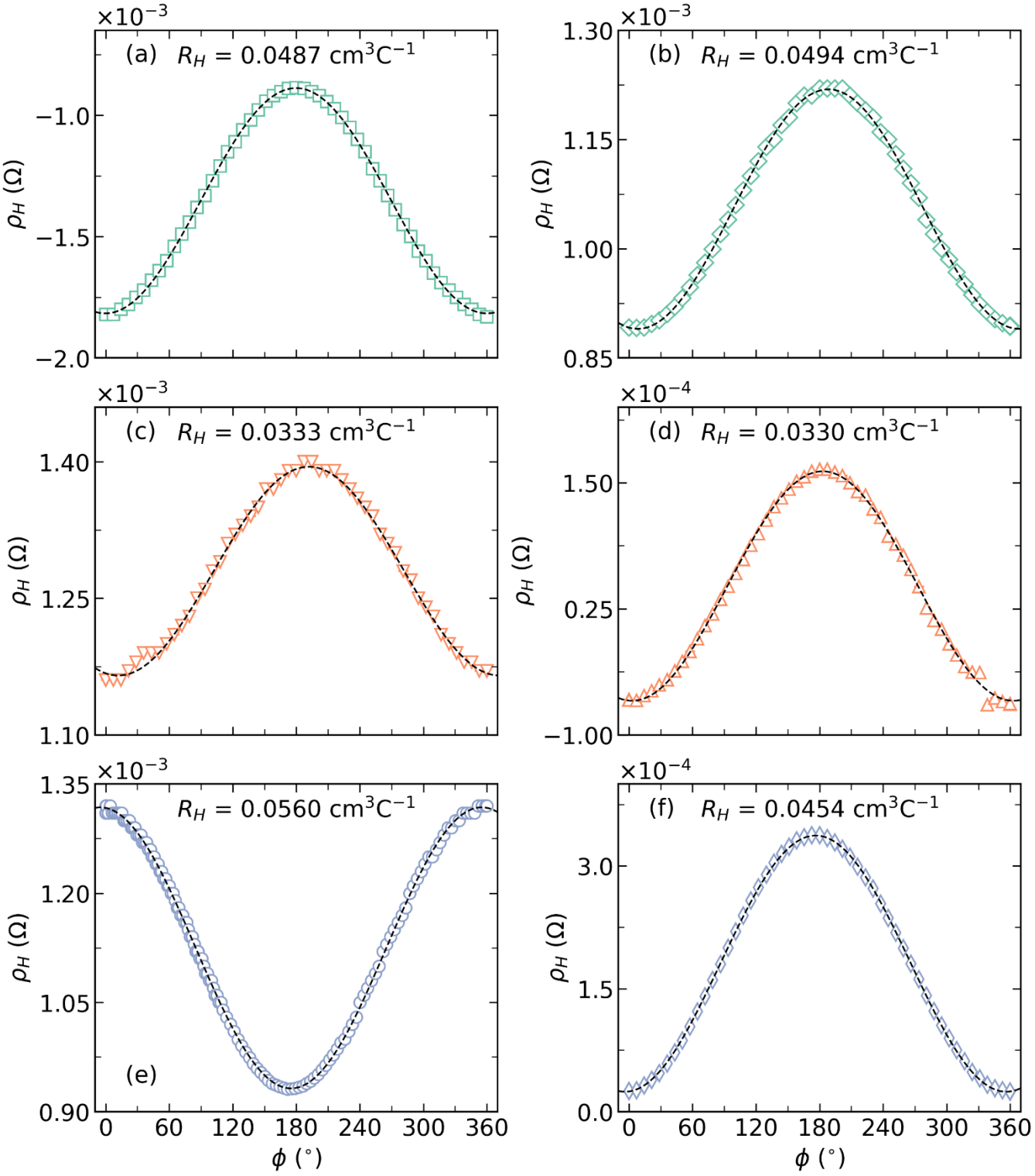

Figure S15. Angular dependence of the Hall resistance in a magnetic field of 1 T for the (a) BMG, (b) BMAG, (c) MS, (d) MSA, (e) BM, and (f) BMA samples. Empty symbols are the experimentally measured points; black dashed lines are the fit with harmonic sine law $\rho_H(\varphi) = \rho_{H0} + \rho_{H1}\sin(\varphi - \varphi_0)$, $R_H = \rho_{H1}/H$.

Charge carrier concentration and mobility; comparison with previous reports

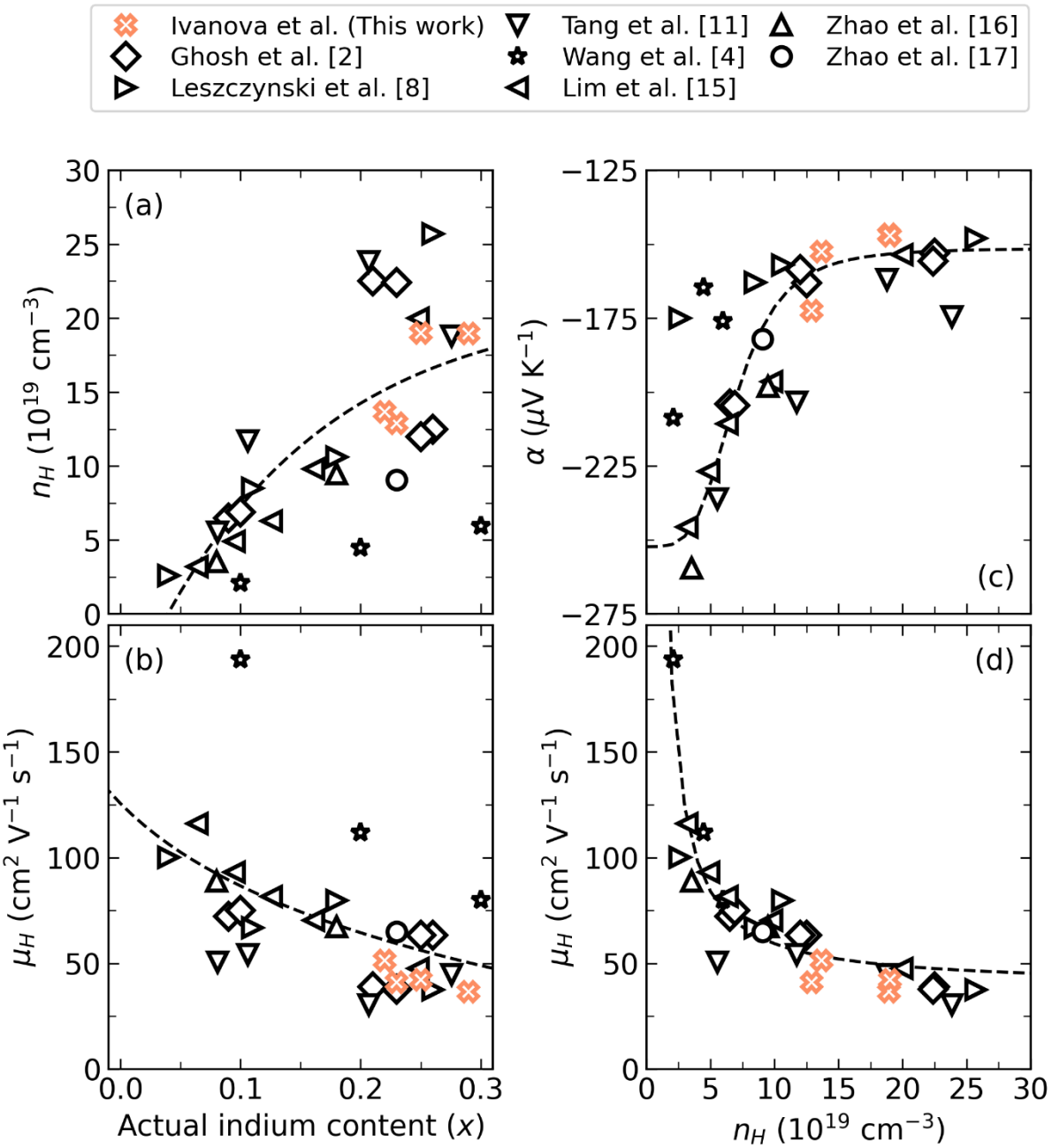

Figure S16. (a) Carrier concentration, n, and (b) carrier mobility, μ, as a function of actual In content in the Co_4Sb_{12} matrix. (c) Seebeck coefficient, α, and (d) carrier mobility, μ, as a function of charge carrier concentration. The orange crosses represent data for the $In_1Co_4Sb_{12+\delta}$ samples obtained in this work (MS, MSA, BMG, and BMAG routes) and for other In-filled $CoSb_3$ skutterudites presented here for comparison.[2,4,8,11,15–17] Black dashed lines are the guides for the eye.

Notes and references

(1) Khovaylo, V.V.; Korolkov, T.A.; Voronin, A.I.; Gorshenkov, M.V.; Burkov, A.T. Rapid Preparation of $In_xCo_4Sb_{12}$ with a Record-Breaking *ZT* = 1.5: The Role of the In Overfilling Fraction Limit and Sb Overstoichiometry. *J. Mater. Chem. A* **2017**, *5* (7), 3541–3546. https://doi.org/10.1039/C6TA09092C.

(2) Ghosh, S.; Meledath Valiyaveettil, S.; Shankar, G.; Maity, T.; Chen, K.-H.; Biswas, K.; Suwas, S.; Mallik, R. C. Enhanced Thermoelectric Properties of In-Filled Co_4Sb_{12} with InSb Nanoinclusions. *ACS Appl. Energy Mater.* **2020**, *3* (1), 635–646. https://doi.org/10.1021/acsaem.9b01851.

(3) Deng, L.; Jia, X.P.; Su, T.C.; Zheng, S.Z.; Guo, X.; Jie, K.; Ma, H.A. The Thermoelectric Properties of $In_xCo_4Sb_{12}$ Alloys Prepared by HPHT. *Mater. Lett.* **2011**, *65* (19–20), 2927–2929. https://doi.org/10.1016/j.matlet.2011.06.002.

(4) Wang, L.; Cai, K.F.; Wang, Y.Y.; Li, H.; Wang, H.F. Thermoelectric Properties of Indium-Filled Skutterudites Prepared by Combining Solvothermal Synthesis and Melting. *Appl. Phys. A* **2009**, *97* (4), 841–845. https://doi.org/10.1007/s00339-009-5329-5.

(5) Gostkowska-Lekner, N.; Trawinski, B.; Kosonowski, A.; Bochentyn, B.; Lapinski, M.; Miruszewski, T.; Wojciechowski, K.; Kusz, B. New Synthesis Route of Highly Porous $In_xCo_4Sb_{12}$ with Strongly Reduced Thermal Conductivity. *J. Mater. Sci.* **2020**, *55* (28), 13658–13674. https://doi.org/10.1007/s10853-020-04952-5.

(6) Gharleghi, A.; Hung, P.-C.; Lin, F.-H.; Liu, C.-J. Enhanced *ZT* of $In_xCo_4Sb_{12}$–InSb Nanocomposites Fabricated by Hydrothermal Synthesis Combined with Solid–Vapor Reaction: A Signature of Phonon-Glass and Electron-Crystal Materials. *ACS Appl. Mater. Interfaces* **2016**, *8* (51), 35123–35131. https://doi.org/10.1021/acsami.6b09026.

(7) He, T.; Chen, J.; Rosenfeld, H.D.; Subramanian, M.A. Thermoelectric Properties of Indium-Filled Skutterudites. *Chem. Mater.* **2006**, *18* (3), 759–762. https://doi.org/10.1021/cm052055b.

(8) Leszczynski, J.; Da Ros, V.; Lenoir, B.; Dauscher, A.; Candolfi, C.; Masschelein, P.; Hejtmanek, J.; Kutorasinski, K.; Tobola, J.; Smith, R.I.; Stiewe, C.; Müller, E. Electronic Band Structure, Magnetic, Transport and Thermodynamic Properties of In-Filled Skutterudites $In_xCo_4Sb_{12}$. *J. Phys. D. Appl. Phys.* **2013**, *46* (49), 495106. https://doi.org/10.1088/0022-3727/46/49/495106.

(9) Mallik, R.C.; Stiewe, C.; Karpinski, G.; Hassdorf, R.; Müller, E. Thermoelectric Properties of Co_4Sb_{12} Skutterudite Materials with Partial In Filling and Excess In Additions. *J. Electron. Mater.* **2009**, *38* (7), 1337–1343. https://doi.org/10.1007/s11664-009-0663-0.

(10) Sesselmann, A.; Dasgupta, T.; Kelm, K.; Müller, E.; Perlt, S.; Zastrow, S. Transport Properties and Microstructure of Indium-Added Cobalt–Antimony-Based Skutterudites. *J. Mater. Res.* **2011**, *26* (15), 1820–1826. https://doi.org/10.1557/jmr.2011.102.

(11) Tang, Y.; Qiu, Y.; Xi, L.; Shi, X.; Zhang, W.; Chen, L.; Tseng, S.-M.; Chen, S.; Snyder, G.J. Phase Diagram of In–Co–Sb System and Thermoelectric Properties of In-Containing Skutterudites. *Energy Environ. Sci.* **2014**, *7* (2), 812–819. https://doi.org/10.1039/C3EE43240H.

(12) Visnow, E.; Heinrich, C.P.; Schmitz, A.; de Boor, J.; Leidich, P.; Klobes, B.; Hermann, R.P.; Müller, W.E.; Tremel, W. On the True Indium Content of In-Filled Skutterudites. *Inorg. Chem.* **2015**, *54* (16), 7818–7827. https://doi.org/10.1021/acs.inorgchem.5b00799.

(13) Le Tonquesse, S.; Alleno, É.; Demange, V.; Prestipino, C.; Rouleau, O.; Pasturel, M. Reaction Mechanism and Thermoelectric Properties of $In_{0.22}Co_4Sb_{12}$ Prepared by Magnesiothermy. *Mater. Today Chem.* **2020**, *16*, 100223. https://doi.org/10.1016/j.mtchem.2019.100223.

(14) Benyahia, M.; Ohorodniichuk, V.; Leroy, E.; Dauscher, A.; Lenoir, B.; Alleno, E. High Thermoelectric Figure of Merit in Mesostructured $In_{0.25}Co_4Sb_{12}$ *n*-Type Skutterudite. *J. Alloys Compd.* **2018**, *735*, 1096–1104. https://doi.org/10.1016/j.jallcom.2017.11.195.

(15) Lim, Y.S.; Park, K.-H.; Tak, J.Y.; Lee, S.; Seo, W.-S.; Park, C.-H.; Kim, T.H.; Park, P.; Kim, I.-H.; Yang, J. Colligative Thermoelectric Transport Properties in *n*-Type Filled $CoSb_3$ Determined by Guest Electrons in a Host Lattice. *J. Appl. Phys.* **2016**, *119* (11), 115104. https://doi.org/10.1063/1.4944434.

(16) Zhao, W.; Wei, P.; Zhang, Q.; Peng, H.; Zhu, W.; Tang, D.; Yu, J.; Zhou, H.; Liu, Z.; Mu, X.; He, D.; Li, J.; Wang, C.; Tang, X.; Yang, J. Multi-Localization Transport Behaviour in Bulk Thermoelectric Materials. *Nat. Commun.* **2015**, *6* (1), 6197. https://doi.org/10.1038/ncomms7197.

(17) Zhao, W.Y.; Dong, C.L.; Wei, P.; Guan, W.; Liu, L.S.; Zhai, P.C.; Tang, X.F.; Zhang, Q.J. Synthesis and High Temperature Transport Properties of Barium and Indium Double-Filled Skutterudites $Ba_xIn_yCo_4Sb_{12-z}$. *J. Appl. Phys.* **2007**, *102* (11), 113708. https://doi.org/10.1063/1.2821364.